Thermal conductivity of $Si_{1-x}Ge_x/Si_{1-y}Ge_y$ superlattices: Competition between interfacial and internal scattering

Z. Aksamija*
Department of Electrical and Computer Engineering, University of Massachusetts–Amherst, Amherst, Massachusetts 01003-9292, USA

I. Knezevic†
Department of Electrical and Computer Engineering, University of Wisconsin–Madison, Madison, Wisconsin 53706-1691, USA

(Received 23 April 2013; revised manuscript received 3 July 2013; published 22 October 2013)

We investigate thermal transport in Si/Ge and $Si_{1-x}Ge_x/Si_{1-y}Ge_y$ alloy superlattices based on solving the single-mode phonon Boltzmann transport equation in the relaxation-time approximation and with full phonon dispersions. We derive an effective interface scattering rate that depends both on the interface roughness (captured by a wave-vector-dependent specularity parameter) and on the efficiency of internal scattering mechanisms (mass-difference and phonon-phonon scattering). We provide compact expressions for the calculations of in-plane and cross-plane thermal conductivities in superlattices. Our numerical results accurately capture both the observed increase in thermal conductivity as the superlattice period increases and the in-plane vs cross-plane anisotropy of thermal conductivity. Owing to the combined effect of interface and internal scattering, an alloy/alloy superlattice has a lower thermal conductivity than bulk SiGe with the same alloy composition. Thermal conductivity can be minimized by growing short-period alloy/alloy superlattices or $Si/Si_{1-x}Ge_x$ superlattices with the SiGe layer thicker than the Si one.

DOI: 10.1103/PhysRevB.88.155318 PACS number(s): 63.22.Np, 63.20.K−, 66.70.−f

I. INTRODUCTION

Silicon, a cheap and widely available semiconductor material, is the basis of modern electronics. However, silicon is not a good thermoelectric material in its bulk form because of its low thermoelectric conversion efficiency. Thermoelectric efficiency is given by a dimensionless figure of merit (ZT), which depends on the Seebeck coefficient (S; also known as the thermopower), absolute temperature (T), and ratio of electrical (σ)-to-thermal conductivity (κ) through $ZT = S^2\sigma T/\kappa$.[1] In most semiconductors, the lattice contribution to thermal conductivity (κ_l) far outweighs its electronic counterpart (κ_e). The high lattice thermal conductivity of bulk silicon at room temperature (146 W/m·K)[2,3] limits the ZT of silicon to approximately 0.05,[4] which is almost two orders of magnitude below $ZT = 3$, the value generally considered desirable in order for solid-state thermoelectric devices to replace the conventional methods of cooling and power generation.[5]

Nanostructuring[6,7] and alloying[8,9] have both been proposed as avenues to boost ZT and improve the thermoelectric conversion efficiency of semiconductors.[10–12] Superlattices offer the possibility of combining quantum confinement in the thin layers of the superlattice with reduced thermal conductivity arising from both nanostructuring and alloying. Bismuth-based superlattices have been shown to possess very high figures of merit, reaching $ZT \approx 2.6$;[13] however, silicon-based superlattices are more attractive from the viewpoint of their lower cost, wider availability, and well-established processing. In addition, silicon-based superlattices offer the ease of integration with existing microelectronics, opening up the possibility for on-chip cooling and improved thermal management in ultrascaled CMOS circuits.[14–16]

Silicon/germanium (Si/Ge)[17] and silicon/alloy ($Si/Si_{1-x}Ge_x$) superlattices[18,19] show promise for application as efficient thermoelectrics because of their low thermal conductivity, below that of bulk $Si_{1-x}Ge_x$ alloys.[20] Initial studies and models of the lattice thermal conductivity in superlattice systems focused primarily on the lattice dynamics and the effect of periodicity on the phonon velocity.[21–23] Models based on the lattice dynamics of the heterostructure are typically limited to having only a few monolayers of each material. In addition, it was found that the reduction in thermal conductivity from the effect of the intrinsic reduction in phonon group velocity due to phonon confinement and coherent reflections at interfaces in superlattices is not enough to account for the measurements[24–26] and that the intrinsic effects lead to a thermal conductivity decreasing with increasing period thickness, opposite to the trends observed in measurements.[27]

Instead, lattice thermal conductivity (especially cross-plane) in thin superlattices appears to be dominated by scattering from the rough interfaces between layers.[22,28,29] In recent years, considerable theoretical work based on density functional theory[30–33] and molecular dynamics[34–37] has addressed thermal transport in semiconductor materials including Si, Ge, SiGe alloys, and Si/Ge superlattices, in particular, issues such as interface conductance[35] and the role of interface scattering in the experimentally observed dependence of thermal conductivity on superlattice period.[30] Intrinsic thermal conductivities based on exact solutions to the PBTE have also been calculated using iterative[32] and variational[33] approaches; however, such approaches are most appropriate for bulk crystals, where size effects arising from boundary scattering can be treated as an additional relaxation time, ignoring any explicit spatial variation in the solution. In contrast, SiGe-alloy-based superlattices,[18,19,38] in which both composition and layer thickness can be used to tune thermal transport,[39,40] have received little theoretical attention.

In this paper, we elucidate the interplay between internal and interface scattering in Si/Ge and SiGe-alloy-based superlattices. Based on solving the phonon Boltzmann transport equation (PBTE) in the usual single-mode, relaxation-time

approximation (RTA), we derive an effective interface scattering rate for a superlattice, which depends on the scattering rate due to internal scattering mechanisms: a complex interdependence between the probability of scattering from a rough interface (captured through a wave-vector-dependent specularity parameter) and the efficiency of internal scattering mechanisms determines the overall influence of interfaces on phonon transport. We also discuss the influence of the random variation of roughness between superlattice layers and determine that the exponential distribution of roughness rms heights over layers works best for capturing experimental measurements, especially the in-plane vs cross-plane anisotropy of the thermal conductivity. We give compact expressions for the calculations of the in-plane and cross-plane thermal conductivities of superlattices that accurately capture the interplay of internal and interface scattering. We compare the results to the measurements in Refs. 17–19 and 41 and demonstrate their excellent agreement. The presented model accurately captures the trend of thermal conductivity increase with superlattice period increase. We also demonstrate that an alloy superlattice has a lower thermal conductivity than bulk SiGe with the same alloy composition. The lowest thermal conductivities can be obtained in alloy superlattices with very thin layers. Also, the model accurately captures the in-plane versus cross-plane anisotropy that has been experimentally demonstrated.

The paper is organized as follows: in Sec. II, we consider phonon transport in bulk alloys. In Sec. III, we present the phonon transport model in layered superlattices, discuss the calculation of the interface scattering rate, and elaborate on the momentum-dependent specularity parameter for the treatment of interface scattering. We also discuss the anisotropy between in-plane and cross-plane thermal transport in superlattices. In Sec. IV, we present the lattice thermal conductivity results for cross-plane transport in Si/Ge and $Si/Si_{1-x}Ge_x$ superlattices and compare them to measurements in Refs. 17–19 and 41. We conclude in Sec. V, with a brief summary and a few final remarks.

II. PHONON TRANSPORT IN BULK ALLOYS

Lattice heat conduction is determined by the phonon distribution function. The steady-state distribution function of phonons can be obtained by solving the time-independent PBTE. In an infinite bulk crystal, no boundaries or interfaces are present. Internal scattering mechanisms (mass-difference scattering from isotopes, alloying, and other impurities such as dopants,[42] anharmonic scattering due to resistive umklapp three-phonon processes,[43] and scattering from any defects present in the crystal[44]) randomize the phonon momentum and relax the distribution function.

In the single-mode RTA, the time-independent PBTE is[45]

$$\vec{v}_b(\vec{q})\cdot\nabla_{\vec{r}}N_b(\vec{q},\vec{r}) = \frac{N_b(\vec{q},\vec{r}) - N^0_{b,T}(\vec{q})}{\tau_{b,\,\mathrm{Internal}}(\vec{q})}. \tag{1}$$

Here, $\vec{q}$ denotes the phonon wave vector, $\vec{v}_b(\vec{q})$ is the phonon velocity, $N_b(\vec{q},\vec{r})$ is the steady-state phonon distribution function, and $N^0_{b,T}(\vec{q})$ is the equilibrium (Bose-Einstein) phonon distribution function at temperature T. The equations hold for each branch b and interbranch scattering is included in $\tau^{-1}_{b,\,\mathrm{Internal}}(\vec{q})$, the scattering rate due to all the intrinsic scattering mechanisms combined:

$$\tau^{-1}_{b,\mathrm{Internal}}(\vec{q}) = \tau^{-1}_{b,U}(\vec{q}) + \tau^{-1}_{b,\mathrm{Impurity}}(\vec{q}) + \tau^{-1}_{b,\mathrm{Alloy}}(\vec{q}). \tag{2}$$

Here, $\tau^{-1}_{b,U}$, $\tau^{-1}_{b,\mathrm{Impurity}}$, and $\tau^{-1}_{b,\mathrm{Alloy}}$ are the umklapp, impurity, and alloy (mass-difference) scattering rates, respectively. Details on the calculation of these rates, which are fairly standard, can be found in the Appendix.

Out of equilibrium, we can write

$$N_b(\vec{q},\vec{r}) = N^0_{b,T}(\vec{q}) + n_b(\vec{q},\vec{r}), \tag{3}$$

so the PBTE becomes

$$\vec{v}_b(\vec{q})\cdot\nabla_{\vec{r}}T\frac{\partial N^0_{b,T}(\vec{q})}{\partial T} + \vec{v}_b(\vec{q})\cdot\nabla_{\vec{r}}n_b(\vec{q},\vec{r}) = \frac{n_b(\vec{q},\vec{r})}{\tau_{b,\,\mathrm{Internal}}(\vec{q})}. \tag{4}$$

In the case of a uniform bulk crystal subject to a small and uniform temperature gradient,

$$\vec{v}_b(\vec{q})\cdot\nabla_{\vec{r}}T\frac{\partial N^0_{b,T}(\vec{q})}{\partial T} = \frac{n_b(\vec{q},\vec{r})}{\tau_{b,\,\mathrm{Internal}}(\vec{q})}. \tag{5}$$

The bulk-limit form of $n_b(\vec{q},\vec{r})$ is denoted $R_b(\vec{q})$ and is given by

$$R_b(\vec{q}) = \tau_{b,\,\mathrm{Internal}}(\vec{q})\vec{v}_b(\vec{q})\cdot\nabla_{\vec{r}}T\frac{\partial N^0_{b,T}(\vec{q})}{\partial T}. \tag{6}$$

A. Thermal conductivity tensor

The full thermal conductivity tensor $\kappa^{\alpha\beta}$ is obtained as a sum over all phonon momenta and branches,[43]

$$\kappa^{\alpha\beta} = \sum_{b,\vec{q}} \tau_b(\vec{q})C_{b,T}(\vec{q})v^\alpha_b(\vec{q})v^\beta_b(\vec{q}), \tag{7}$$

where $\tau_b(\vec{q})$ is the total phonon relaxation time [for a bulk sample, $\tau_b(\vec{q}) = \tau_{b,\mathrm{Internal}}(\vec{q})$ from Eq. (2)] and the phonon heat capacity per mode $C_{b,T}(\vec{q})$ is given by

$$C_{b,T}(\vec{q}) = \frac{[\hbar\omega_b(\vec{q})]^2}{k_BT^2}\frac{e^{(\hbar\omega_b(\vec{q})/k_BT)}}{[e^{(\hbar\omega_b(\vec{q})/k_BT)}-1]^2}. \tag{8}$$

$v^\alpha_b(\vec{q})$ is a component of the phonon velocity vector calculated from the full phonon dispersion based on Weber's adiabatic bond charge (ABC) model.[46] The ABC model includes interactions between ions, bond charges, bond bending, and long-range electrostatic interactions and has been shown to reproduce measured phonon vibrational frequencies in virtually all group IV,[46–49] III–V,[49,50] and II–VI[51] semiconductors with excellent accuracy. The ABC phonon dispersions for Si can be found in Refs. 46 and 47, and those for Ge in Refs. 46 and 49. Vibrational properties of $Si_{1-x}Ge_x$ alloys, including phonon dispersion and velocity, are calculated here in the virtual crystal approximation.[20]

Figure 1 shows the thermal conductivity of bulk SiGe alloys as a function of composition. The strong quadratic dependence on the germanium fraction x, especially in Γ_{Mass}, is the primary reason for the drastic reduction in thermal conductivity from pure Si or Ge to the alloy. The thermal conductivity of bulk alloys quickly decreases for low concentrations and then reaches a wide and nearly flat plateau for $0.2 < x < 0.8$.

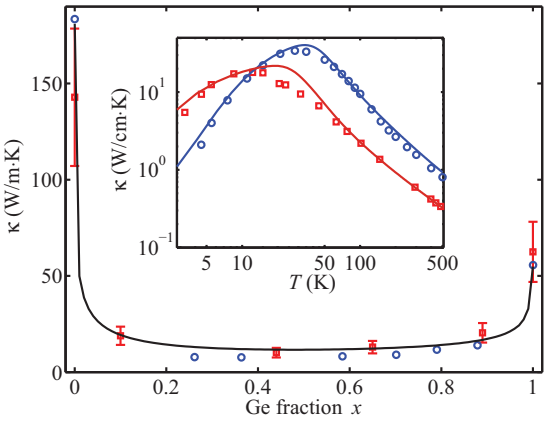

FIG. 1. (Color online) Thermal conductivity of bulk $Si_{1-x}Ge_x$, showing a strong dependence on the germanium fraction x. The thermal conductivity of bulk alloys quickly decreases with increasing x, then reaches a plateau for $0.2 < x < 0.8$. Experimental data points are shown for comparison, demonstrating excellent agreement with the model. The (blue) circles are taken from Ref. 52, and the (red) squares from Ref. 39. Inset: The calculated thermal conductivity shows excellent agreement with the measurements from Ref. 2 for bulk Si [(blue) circles] and Ge [(red) squares] over a wide range of temperatures.

Experimental data points are shown for comparison,[39,52] demonstrating excellent agreement between measured bulk alloy thermal conductivities and the model.

III. PHONON TRANSPORT MODEL FOR ALLOY SUPERLATTICES

There are two types of models traditionally used to describe the transport of phonons across the interface between different materials. One is the acoustic mismatch model (AMM), originally proposed by Khalatnikov[53] to describe the experiments by Kapitza on the copper/helium thermal boundary.[54] In the acoustic mismatch model, the interface is essentially viewed as perfectly smooth and phonons are treated as classical waves, whose transmission and reflection obey a generalization of Snell's law. While this view is valid for long-wavelength (zone-center) phonons, it is inadequate for shorter-wavelength phonons,[55–57] which scatter strongly from the atomically rough interface features. The diffuse mismatch model (DMM)[58] treats the interface as perfectly diffuse: a phonon is destroyed at the interface and the replacement phonon's probability of transmission to either side of the interface depends on the ratio of the density of phonon states in the two media.

In this section, our goal is to develop a model that will accurately predict both the cross-plane and the in-plane transport in realistic superlattices, where layers are generally acoustically mismatched and the interfaces are always atomically rough. We wish to go beyond the diffuse mismatch model and allow for partially (as opposed to completely) diffuse scattering at the interfaces, to seek a model that will account for different phonon modes seeing the surface roughness features differently. It is important to note that we do not assume to be working with superlattices whose periods are so small and interfaces so smooth and so well acoustically matched that wave effects become significant and miniband formation due to periodicity and essentially ballistic phonon transport are observed. The model developed here is firmly in the domain of semiclassical (Boltzmann) phonon transport, applicable to superlattices whose layer thicknesses are comparable to or longer than the phonon mean free path, which will occur in two types of systems: in bulklike SiGe-based superlattices, where the layer thickness (and consequently the lattice period) exceeds the mean free path due to internal scattering and the dominant internal scattering mechanism (typically alloy scattering; see Fig. 1) governs transports; and in short-period superlattices with interface roughness, where layers are thinner than the mean free path for internal scattering, and the total phonon mean free path will approximately equal the layer thickness due to phonon scattering at the rough interfaces.[28]

The following two limits reveal some important considerations that inform our model.

1. Acoustic mismatch, but no interface roughness. Assume that we have a single interface between two slabs of acoustically mismatched materials. If we were to let the surface roughness vanish, the remaining interface effects would be due to acoustic mismatch alone. Now, assume that we put a thermal contact on each of the two slabs, so that heat flows across the interface when the two contacts are held at different temperatures. As there are no diffusive processes at the interface, the populations of individual phonon modes would be dictated by the diffusive processes in each slab; each slab would thermalize individually. In the steady state, each bulklike slab will reach a constant temperature, but, in order to accommodate the flux across the interface, there will be a temperature step at the interface. This scenario reveals the existence of an interface resistance between mismatched materials because, in order to accommodate the nonzero heat flux, the populations of phonons that are connected via Snell's law on the two sides of the interface deviates from the detailed balance that holds across the interface in equilibrium.

In contrast, if we put two thermal contacts at different temperatures in one of the directions parallel to the interface, so that heat flows parallel to the interface, thermal conductivity would coincide with the thermal conductivity of the two slabs in parallel. With no flux across the interface, there would be no temperature step across the interface and the relative populations of the modes that are connected on the two sides of the interfaces would remain the same as in equilibrium, i.e., satisfy detailed balance at every point along the interface.[58,59]

The conclusion is that the effect of pure acoustic mismatch should definitely be captured at the level of cross-plane thermal conduction, but not in-plane conduction. In addition, mismatch at the interface does not lead to randomization of the phonon momentum; instead, mismatch only leads to partial transmission of the phonon wave, without randomizing its direction.[60] Hence, mismatch should not be captured at the level of a scattering mechanism in the solution of the PBTE because the thermal conductivity tensor obtained from the solution to the PBTE applies equally in both the in-plane and the cross-plane transport directions. Instead, interface mismatch should be captured through an additional resistance at the interface in the case of cross-plane thermal transport.[61]

2. Rough interface, no acoustic mismatch. Now, imagine the case in which we have two acoustically matched layers, separated by a rough interface (for instance, a grain boundary between two misoriented grains in a polycrystalline material). Each time a phonon is about to cross the rough interface, there is a finite probability p that it will go through unscattered and the complementary probability $1-p$ that its momentum will be randomized. An unscattered phonon contributes appreciably to the population of that same mode on the other side of the interface, therefore the effect of scattering from roughness should be observable at the level of phonon distribution. Indeed, in the presence of rough interfaces and the corresponding effects in phonon distributions, both cross-plane and in-plane thermal conductivity will be affected, as observed in experiments.[62,63]

While in reality it is certainly true that one cannot separate an atomically rough interface between two materials from the actual materials, this is effectively what we do here in order to arrive at a tractable model that satisfies physical limits 1 and 2 above. We treat surface roughness and acoustic mismatch separately, in the following sense: the interface roughness is captured at the level of phonon distributions, i.e., it is incorporated into the solution to the PBTE, while acoustic mismatch is captured at the level of thermal conductivity calculation, through an additional acoustic-mismatch interface resistance.[58,64]

A. Brief overview and key features of the phonon transport model

We consider a superlattice consisting of materials 1 and 2, with layers of thicknesses L_1 and L_2, respectively. All interfaces between them are rough, with a characteristic distribution of roughness rms heights, and we assume that, on average, we can characterize each interface with the same effective rms roughness and thus the same momentum-dependent specularity parameter $p(\vec{q})$ (see more in Sec. III D). If we forget about acoustic mismatch, we can think of the layers of the superlattice as interspersed layers of two sublattices, one consisting of material 1 only and the other consisting of material 2 only, each sublattice having rough interfaces between adjacent layers. We calculate the thermal conductivity tensors of the two sublattices, each with layers of a single thickness (L_1 or L_2), based on solving the PBTE with partially diffuse interface scattering (Sec. III E). Then, cross-plane thermal conductivities of the sublattices are combined in series, with an additional contribution from mismatch-induced interface resistance, while in-plane conductivities are combined in parallel.

The model (i) enables calculation of the full thermal conductivity tensor for a superlattice within a unified framework, (ii) reproduces the measured in-plane versus cross-plane anisotropy, and (iii) reproduces the thickness and alloy composition dependence of the measured cross-plane thermal conductivity. In the rest of this section, we present the technical details of the model.

B. A single interface

Consider the case of a single rough interface between two acoustically matched materials, located at $y=0$. Because of the interface, the crystal is no longer completely uniform, and the phonon density becomes dependent on y, $N_{\mathrm{b}}(\vec{q},y) = N^0_{\mathrm{b},T}(\vec{q}) + n_{\mathrm{b}}(\vec{q},y)$.[42] The steady-state PBTE can be written as

$$\vec{v}_{\mathrm{b}}(\vec{q})\cdot\nabla_{\vec{r}}T\frac{\partial N^0_{\mathrm{b},\vec{q}}(T)}{\partial T} + v_{\mathrm{b},\perp}(\vec{q})\frac{\partial n_{\mathrm{b}}(\vec{q},y)}{\partial y} = \frac{n_{\mathrm{b}}(\vec{q},y)}{\tau_{\mathrm{b,\,Internal}}(\vec{q})}, \tag{9}$$

which we must solve for $n_{\mathrm{b}}(\vec{q},y)$. The solution of Eq. (9) in this case is specified by the boundary condition $n_{\mathrm{b}}(\vec{q},0)$ for the phonon distribution at the interface, while the solution will tend to the bulk RTA solution $R_{\mathrm{b}}(\vec{q})$ away from the interface.[42] Consequently, we can write the complete solution $n_{\mathrm{b}}(\vec{q},y)$ of Eq. (4) as a combination of $n_{\mathrm{b}}(\vec{q},0)$ and the RTA expressions

$$\begin{aligned} n_{\mathrm{b}}(\vec{q},y) = {} & R_{\mathrm{b}}(\vec{q})\{1-\exp[-y/\tau_{\mathrm{b,\,Internal}}(\vec{q})v_{\mathrm{b},\perp}(\vec{q})]\} \\ & + n_{\mathrm{b}}(\vec{q},0^+)\exp[-y/\tau_{\mathrm{b,\,Internal}}(\vec{q})v_{\mathrm{b},\perp}(\vec{q})], \end{aligned} \tag{10}$$

where $\tau_{\mathrm{b,\,Internal}}(\vec{q})v_{\mathrm{b},\perp}(\vec{q})$ is the mean free path in bulk due to internal scattering. The second term in Eq. (10) is the contribution to $n_{\mathrm{b}}(\vec{q},y)$ from all the phonons in the same mode that existed at $y=0^+$ and remained unscattered until they reached y.

The boundary condition $n_{\mathrm{b}}(\vec{q},0^+)$ at an interface is dictated by the interface roughness. The probability that a phonon will pass through the interface unscattered is given by the specularity factor $p(\vec{q})$. For a right-moving phonon (i.e., one moving in the positive y-direction) with momentum $\vec{q}$ and velocity component $v_{\mathrm{b},\perp}(\vec{q})$ perpendicular to the interface, a fraction $p(\vec{q})$ of the $N_{\mathrm{b}}(\vec{q},0^-)$ incoming phonons will be transmitted unscattered, while the remaining $1-p(\vec{q})$ phonons will be diffusely scattered and randomized. We can write the boundary condition at the interface as[65]

$$N_{\mathrm{b}}(\vec{q},0^+) = p(\vec{q})N_{\mathrm{b}}(\vec{q},0^-) + [1-p(\vec{q})]N^0_{\mathrm{b},T}(\vec{q}). \tag{11}$$

[The scattered portion of the solution, given by the the second term on the right-hand side of Eq. (11), relaxes back to the equilibrium phonon distribution.] The first term in Eq. (11) tells us that a fraction $p(\vec{q})$ of the surplus phonons in mode $\vec{q}$ will continue along the path defined by their group velocity $v_{\mathrm{b},\perp}(\vec{q})$; i.e., Eq. (11) can be written as

$$n_{\mathrm{b}}(\vec{q},0^+) = p(\vec{q})n_{\mathrm{b}}(\vec{q},0^-), \tag{12}$$

where $n_{\mathrm{b}}(\vec{q},0^-)$ is the number of phonons in mode b,$\vec{q}$ to the left of the interface.

C. Effective interface scattering rate for a superlattice

Assume we have a superlattice with layers of thickness L. All layers are made of the same material but separated by rough interfaces, and all interfaces have the same scattering properties, i.e., the same specularity parameter $p(\vec{q})$. Under

these assumptions, the purpose of this section is to derive the phonon population inside a single layer.

After a phonon enters a layer at $y = 0$, we can trace its path as in Fig. 2. Every time the phonon reaches an interface, it has probability $p(\vec{q})$ of continuing unscattered into the neighboring layer and probability $1 - p(\vec{q})$ of being scattered diffusely. Inside the layer, the phonon can undergo scattering due to internal scattering mechanisms.

As a result, the phonon distribution at a given y inside the layer carries contributions from phonons that did not cross any interfaces between having been created (as a result of an internal scattering event) and reaching y, along with contributions from all the phonons that were generated in preceding layers and have crossed one, two, three, or more interfaces unscattered in order to reach y. Based on Eqs. (10) and (12), we thus obtain an infinite sum of the form

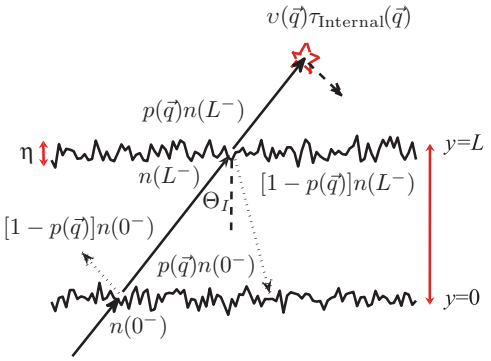

FIG. 2. (Color online) Phonon trajectory inside a single layer of a superlattice. The phonon has probability $p(\vec{q})$ of crossing an interface unscattered and probability $1 - p(\vec{q})$ of scattering and having its momentum randomized. Inside the layer, the phonon's trajectory can be interrupted by internal scattering mechanisms.

$$\begin{aligned} n_b(\vec{q},y) = {} & R_b(\vec{q})[1-\exp(-y/\tau_{b,\,\text{Internal}}(\vec{q})v_{b,\perp}(\vec{q}))] + p(\vec{q})\exp(-y/\tau_{b,\,\text{Internal}}(\vec{q})v_{b,\perp}(\vec{q})) \\ & \times \{R_b(\vec{q})[1-\exp(-L/\tau_{b,\,\text{Internal}}(\vec{q})v_{b,\perp}(\vec{q}))] + p(\vec{q})\exp(-L/\tau_{b,\,\text{Internal}}(\vec{q})v_{b,\perp}(\vec{q})) \\ & \times \{R_b(\vec{q})[1-\exp(-L/\tau_{b,\,\text{Internal}}(\vec{q})v_{b,\perp}(\vec{q}))] + \cdots\}\}. \end{aligned} \tag{13}$$

Here, the term proportional to $p(\vec{q})^m$ describes the contribution from phonons that crossed m interfaces unscattered in order to reach y. Written compactly,

$$n_b(\vec{q},y) = R_b(\vec{q})\left\{1-[1-p(\vec{q})]\exp[-y/\tau_{b,\,\text{Internal}}(\vec{q})v_{b,\perp}(\vec{q})]\sum_{k=0}^{\infty} p(\vec{q})^k \exp[-kL/\tau_{b,\,\text{Internal}}(\vec{q})v_{b,\perp}(\vec{q})]\right\}. \tag{14}$$

The sum can be expressed in closed form as a product of the RTA bulk solution, $R_b(\vec{q})$, and a factor due to the periodic array of partially diffuse interfaces spaced by L:

$$n_b(\vec{q},y) = R_b(\vec{q})\left\{1-\left[\frac{1-p(\vec{q})}{1-p(\vec{q})\exp[-L/\tau_{b,\,\text{Internal}}(\vec{q})v_{b,\perp}(\vec{q})]}\right]\exp[-y/\tau_{b,\,\text{Internal}}(\vec{q})v_{b,\perp}(\vec{q})]\right\}. \tag{15}$$

If we substitute $n_b(\vec{q},y)$ and $R_b(\vec{q})$ from Eq. (6) into Eq. (4), then average the whole equation along the y direction over the layer, we can define an *effective interface scattering rate*, $\tau^{-1}_{\text{Interface}}(\vec{q})$, through[42]

$$\frac{R_b(\vec{q})}{\tau_{b,\,\text{Internal}}(\vec{q})} = \left[\frac{1}{\tau_{b,\,\text{Internal}}(\vec{q})} + \frac{1}{\tau_{\text{Interface}}(\vec{q})}\right]\langle n_b(\vec{q},y)\rangle. \tag{16}$$

Here, $\langle\cdots\rangle$ represents an average over y. The interface scattering rate is then obtained as

$$\frac{1}{\tau_{\text{Interface}}(\vec{q})} = \frac{v_{b,\perp}(\vec{q})}{L}\frac{F_p(\vec{q},L)}{1-\frac{\tau_{b,\,\text{Internal}}(\vec{q})v_{b,\perp}(\vec{q})}{L}F_p(\vec{q},L)}, \tag{17}$$

where a mode-dependent scaling factor $F_p(\vec{q},L)$ is given by

$$F_p(\vec{q},L) = \frac{[1-p(\vec{q})]\{1-\exp[-L/\tau_{b,\,\text{Internal}}(\vec{q})v_{b,\perp}(\vec{q})]\}}{1-p(\vec{q})\exp[-L/\tau_{b,\,\text{Internal}}(\vec{q})v_{b,\perp}(\vec{q})]}. \tag{18}$$

This formulation of interface scattering allows for the rates of internal and interface scattering to be added together,[66] despite their interdependence. The factor given by Eq. (18) encapsulates the competition between interface and internal scattering: the effective strength of interface scattering will depend on the strength of the competing internal scattering mechanisms. There are two extremes to this effect. When internal scattering is very strong, such as in alloy layers of a superlattice, the internal scattering mechanisms will tend to minimize the effect of the interfaces, which results in the interface scattering rate being reduced to a simpler form (limit $\tau_{b,\,\text{Internal}} \to 0$),

$$\frac{1}{\tau_{\text{Interface}}(\vec{q})} = \frac{v_{b,\perp}(\vec{q})}{L}[1-p(\vec{q})]. \tag{19}$$

On the opposite extreme, where interface scattering is strongly dominant (as in the case of pure crystal layers thinner than the mean free path for internal scattering), internal scattering can be considered very weak ($\tau_{b,\,\text{Internal}} \to \infty$). In this limit, the interface scattering rate reduces to the well-known expression derived by Ziman,[67]

$$\frac{1}{\tau_{\text{Interface}}(\vec{q})} = \frac{2v_{b,\perp}(\vec{q})}{L}\frac{1-p(\vec{q})}{1+p(\vec{q})}, \tag{20}$$

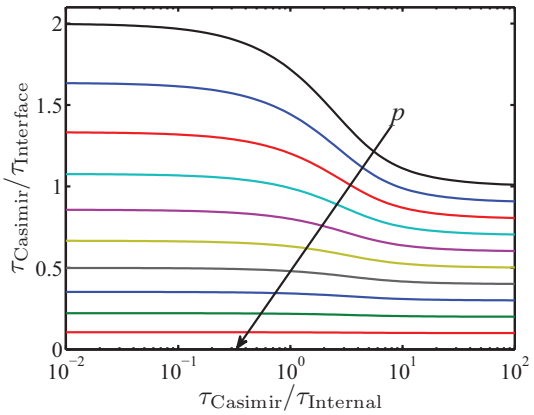

FIG. 3. (Color online) Interface scattering rate versus internal scattering rate [both rates are given in units of the Casimir rate, $\upsilon_{b,\perp}(\vec{q})/L$] for values of the specularity parameter $p(\vec{q})$ ranging from 0.1 to 1, in 0.1 increments. The direction of increasing $p(\vec{q})$ is marked by the arrow. Increasing specularity decreases the overall rate of interface scattering, as well as the competition between interface and internal scattering mechanisms. In the diffuse case (smaller p), there is a larger variation in the interface scattering rate due to competing internal scattering. Overall, the maximum variation due to competition between interface and internal scattering can account for a factor of 2 difference in the interface scattering rate.

with the additional factor of 2 due to the two-dimensional slab geometry of a single layer (the ratio of perimeter length to cross-sectional area of a slab of thickness L is $P/A = 2/L$ in the limit of a very thin slab).[68]

The behavior of the internal scattering rate between the two extremes is shown in Fig. 3, where we plot the value of the interface scattering rate $\tau^{-1}_{\text{Interface}}(\vec{q})$ [in units of the "Casimir" rate $\tau^{-1}_{\text{Casimir}}(\vec{q}) = \upsilon_{b,\perp}(\vec{q})/L$] as a function of the internal scattering rate $\tau^{-1}_{\text{b, Internal}}(\vec{q})$ in the same units. We can see the limit where interface scattering dominates on the left, and the opposite limit where internal scattering dominates on the right side of the plot. Overall, the variation in the internal scattering rate can be a factor of 2 for the completely diffuse case [$p(\vec{q}) = 0$], but this variation decreases for more specular interfaces, where $p(\vec{q})$ is closer to 1.

D. Effective specularity parameter for a superlattice

Previous calculations relied on treating the interface scattering with an empirical specularity parameter, which is then either assumed to be zero[66] (corresponding to completely diffuse interfaces) or adjusted empirically to fit experiments.[59,69,70] In our model, in order to accurately treat phonon scattering from a series of atomically rough interfaces with different roughness rms heights η, we employ the momentum-dependent specularity parameter $p(\vec{q})$. If all interfaces had the same rms roughness height, we could describe the entire superlattice with a single $p(\vec{q})$; however, since the rms heights η of the rough interfaces will be randomly distributed around an average rms height Δ, we must describe the rms roughness heights of all the interfaces in a superlattice by a probability distribution function $P(\eta)$.[71] The probability distribution of interface roughness heights is not known *a priori*; however, we can choose a suitable distribution function based on a small set of reasonable assumptions. The roughness heights of the superlattice interfaces are uncorrelated, but they are similar because the same process is used repeatedly in all layers of the superlattice. We expect that the distribution function $P(\eta)$ should therefore go smoothly to 0 in the limit of $\eta = \infty$ and should have an average value given by a single parameter—the average, or effective, rms interface roughness height Δ. These criteria are well satisfied by several standard distributions, namely, the exponential,[71,72] the half-normal, and the Rayleigh distribution, given by

$$P_{\text{exp.}}(\eta) = \frac{1}{\Delta}\exp\left(-\frac{\eta}{\Delta}\right), \tag{21a}$$

$$P_{\text{hfn.}}(\eta) = \frac{2}{\pi\Delta}\exp\left(-\frac{\eta^2}{\pi\Delta^2}\right), \tag{21b}$$

$$P_{\text{ray.}}(\eta) = \frac{\pi\eta}{2\Delta^2}\exp\left(-\frac{\pi\eta^2}{4\Delta^2}\right). \tag{21c}$$

All three distributions have Δ as their mean.

The effective value of the specularity parameter $\bar{p}(\vec{q})$ is then obtained from the momentum-dependent specularity parameter for a single interface,[47] $p(\vec{q}) = \exp(-4\eta^2 q^2\cos^2\Theta_I)$, by averaging over the distribution of interfaces present between the layers of the superlattice. This is achieved by integrating the single-interface specularity parameter $p(\vec{q})$ over the probability distribution function $P(\eta)$ of the rms roughness heights of the individual interfaces:[67,72]

$$\bar{p}(\vec{q}) = \int_0^\infty P(\eta)\exp(-4\eta^2 q^2\cos^2\Theta_I)d\eta. \tag{22}$$

Using Eqs. (21) for $P(\eta)$ and integrating as in Eq. (22), we derive a set of new analytical expressions for the effective specularity parameter $\bar{p}(\vec{q})$ for each of the distributions given in Eqs. (21) as

$$\bar{p}_{\text{exp.}}(\vec{q}) = \frac{\sqrt{\pi}\exp\left(\frac{1}{4\Delta q\cos\Theta_I}\right)\text{erfc}\left(\frac{1}{4\Delta q\cos\Theta_I}\right)}{4\Delta q\cos\Theta_I}, \tag{23a}$$

$$\bar{p}_{\text{hfn.}}(\vec{q}) = \frac{1}{\sqrt{4\pi\Delta^2 q^2\cos^2\Theta_I + 1}}, \tag{23b}$$

$$\bar{p}_{\text{ray.}}(\vec{q}) = \frac{\pi}{16\Delta^2 q^2\cos^2\Theta_I + \pi}, \tag{23c}$$

where erfc is the complementary error function. The expressions in Eqs. (23) allow us to connect the effective specularity parameter $\bar{p}(\vec{q})$ with the average magnitude of the surface roughness height Δ, the phonon wave vector $\vec{q}$, and the angle Θ_I between the incident phonon and the interface surface normal (see the schematic in Fig. 2). By comparing the numerical model for each of the three candidate distributions to measured data, we can select the one that best represents the distribution of roughness heights of the interfaces in a superlattice. In the remainder of this paper, the exponential distribution will be used because it offers the best agreement with measured data.

E. Superlattice thermal conductivity tensor. Interface resistance

To calculate the thermal conductivity tensor of a SiGe-alloy-based superlattice ($Si_{1-x}Ge_x/Si_{1-y}Ge_y$), with layers of thickness L_1 and L_2, respectively, we can think of it as having

interspersed layers of two sublattices: one consisting only of $Si_{1-x}Ge_x$, with layers of thickness L_1, and the other having $Si_{1-y}Ge_y$ layers of thickness L_2. The thermal conductivity tensor of each sublattice can be obtained based on Eq. (7), with the total relaxation rate $\tau_b^{-1}(\vec{q})$ given by the sum of the internal and interface scattering rates,

$$\frac{1}{\tau_b(\vec{q})} = \frac{1}{\tau_{b,\text{Internal}}(\vec{q})} + \frac{1}{\tau_{b,\text{Interface}}(\vec{q})}, \tag{24}$$

where the calculation of $\tau^{-1}_{b,\text{Interface}}(\vec{q})$ is done based on Eq. (17).

Once the thermal conductivity tensors for each of the two alternating layers in the superlattice have been obtained, they are decomposed into their respective in-plane (assumed to be along the x axis) and cross-plane (along the y axis) components, κ^{xx} and κ^{yy}. Note that we are neglecting possible in-plane anisotropy.[47] The two alternating layers of the superlattice are combined in series for cross-plane transport through the superlattice[22] and in parallel for in-plane transport along the plane of the interfaces:[73]

$$\kappa_{\text{in-plane}} = \frac{L_1\kappa_1^{xx} + L_2\kappa_2^{xx}}{L_1 + L_2}, \tag{25a}$$

$$\kappa_{\text{cross-plane}} = \frac{L_1 + L_2}{\frac{L_1}{\kappa_1^{yy}} + \frac{L_2}{\kappa_2^{yy}} + \frac{1}{\sigma_1^{\text{AIM}}} + \frac{1}{\sigma_2^{\text{AIM}}}}, \tag{25b}$$

where $1/\sigma_{1,2}^{\text{AIM}}$ are the additional interface resistance contributions due to the acoustic impedance mismatch between the two materials,[58] one for each interface ($1 \to 2$ and $2 \to 1$). The interface resistance is added to the contribution from partially diffuse scattering in each layer because it arises from the two materials' having different phonon velocity components $v_b^{\perp}(\vec{q})$ normal to the interface and, consequently, different acoustic impedances $Z_{b,i}^{\perp}(\vec{q}) = \rho_i v_{b,i}^{\perp}(\vec{q})$.[70] The interface conductance κ^{AIM} is obtained from the transmission coefficient in the direction perpendicular to the interface,[74]

$$t_b^{\text{AIM}}(\vec{q}) = \frac{4Z_{b,1}^{\perp}(\vec{q})Z_{b,2}^{\perp}(\vec{q})}{[Z_{b,1}^{\perp}(\vec{q}) + Z_{b,2}^{\perp}(\vec{q})]^2}, \tag{26}$$

by summing over all phonon branches b that contribute to transport in each layer $i = 1,2$ and all modes $\vec{q}$ that satisfy the energy transmission $\omega_1(\vec{q}) \leqslant \max_{b,\vec{q}}\omega_2(\vec{q})$ and critical angle $\Theta_I \leqslant \Theta_c$ conditions:[58]

$$\sigma_{i,T}^{\text{AIM}} = \frac{1}{2}\sum_{b,\vec{q}} \frac{C_{i,b,T}(\vec{q})v_{i,b}^{\perp}(\vec{q})t_b^{\text{AIM}}(\vec{q})}{1 - \langle t_b^{\text{AIM}}(\vec{q})\rangle}. \tag{27}$$

The correction factor in the denominator ensures that the interface resistance goes to 0 in the limit of a fictitious ideal interface between two identical materials, where t^{AIM} becomes unity and interface resistance must vanish.[70]

IV. RESULTS: THERMAL CONDUCTIVITY IN ALLOY SUPERLATTICES

In superlattices, the difference between the in-plane and the cross-plane components of the thermal conductivity tensor, Eqs. (25), gives rise to strong in-plane/cross-plane anisotropy in heat transport. The anisotropy is caused by the difference in the effect of interface scattering on in-plane versus cross-plane transport: in the in-plane direction, heat is carried largely by phonons whose velocities are nearly parallel to the interface and which therefore undergo significantly less interface scattering than phonons that carry heat cross-plane.[47] The effect of anisotropy can be seen in Fig. 4, where excellent agreement with the measured data, taken from Ref. 41, is achieved. In choosing the right model for the roughness distribution from among the exponential, half-normal, and Rayleigh distributions, we find that the exponential distribution and $\bar{p}$ given by Eq. (23a) reproduce the experimental data best, in particular, the measured in-plane/cross-plane ratio.

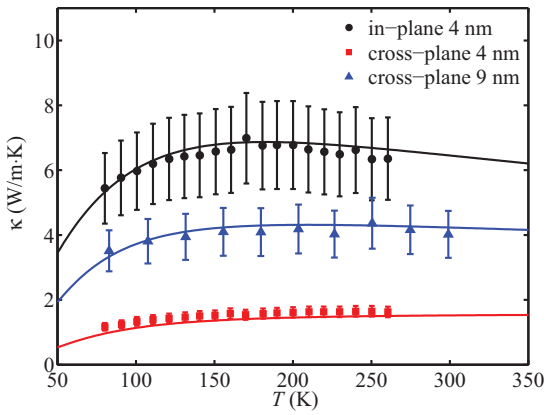

FIG. 4. (Color online) Thermal conductivity of a 9-nm-period Si/Ge superlattice in the cross-plane direction [(blue) triangles] and a 4-nm-period Si/Ge superlattice in both the in-plane [(black) circles] and the cross-plane directions [(red) squares]. Experimental data, represented by symbols, were taken from Refs. 41 and 62. The anisotropy between the in-plane and the cross-plane directions, as well as the thickness and temperature dependence, is well explained by our momentum-dependent interface roughness scattering model.

Results for 4-nm period Si/Ge superlattices in Fig. 4 (data from Ref. 41) show a strong anisotropy of thermal conductivity due to the directional dependence of the phonon velocity and boundary scattering, as discussed above. In addition, interface resistance due to acoustic mismatch only affects cross-plane transport, where heat flux is directed normal to the interfaces. We find that interface resistance due to acoustic impedance mismatch plays a minor role relative to the strong effect of diffuse scattering at the interfaces between successive layers. The effect of acoustic impedance mismatch is strongest in Si/Ge superlattices, due to the larger difference in acoustic wave velocities between the two materials, and the interface resistance $(\kappa^{\text{AIM}})^{-1}$ reaches about 2×10^{-9} m^2 K/W at room temperature, in agreement with previous calculations.[58,75] With increasing germanium fraction in the alloy layers of $Si/Si_{1-x}Ge_x$ and $Si_{1-x}Ge_x/Si_{1-y}Ge_y$ superlattices, the difference in phonon velocities diminishes, further reducing the effect of the acoustic impedance mismatch.

The computed values of cross-plane thermal conductivity $\kappa_{\text{cross-plane}}$ in Fig. 5 show excellent agreement with the measurements on Si/Ge superlattices at both high and low temperatures. Symbols represent the data taken from Ref. 17 for superlattice periods ranging from 3 to 6.5 nm. The rms roughness amplitude Δ was taken as the only adjustable parameter. The value of Δ varies from sample to sample and was assumed to be 1.4 Å in thinner samples with 3- and 5-nm period lengths, while the values of 3 and 1.65 Å were

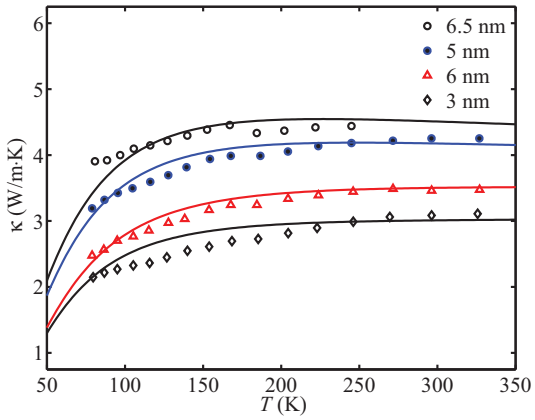

FIG. 5. (Color online) Cross-plane thermal conductivity of Si/Ge superlattices with periods ranging from 3 to 6.5 nm. Experimental data, represented by symbols, was taken from Ref. 17. The general trend is that thermal conductivity increases with superlattice period; however, it also depends on the relative thicknesses of the two constituent materials.

used for thicker samples with period lengths of 6 and 6.5 nm, respectively. We note here that, although the 6-nm superlattice has a larger period thickness, the thermal conductivity is reduced below that of the 5-nm-period superlattice because of the larger value of Δ, showing that partially diffuse scattering at the interfaces can play a dominant role in the lattice thermal conductivity of short-period superlattices.

The computed values of cross-plane thermal conductivity also show excellent agreement with the measurements on a 3.5-μm-thick $Si_{0.9}Ge_{0.1}$ alloy film and 15-nm-period $Si/Si_{0.4}Ge_{0.6}$ superlattices, as shown in Fig. 6. Experimental data, represented by symbols in Fig. 6, were taken from Refs. 18, 76, and 77. The electronic component of thermal

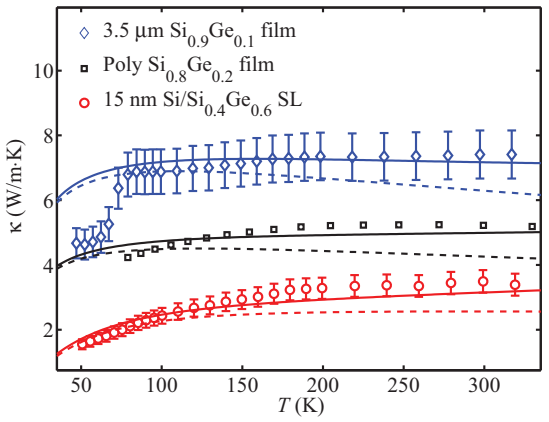

FIG. 6. (Color online) Thermal conductivity of a 3.5-μm $Si_{0.9}Ge_{0.1}$ alloy film [(blue) curve with diamonds], a bulk-sintered $Si_{0.8}Ge_{0.2}$ alloy (black curve with squares), and a 15-nm-period-thickness 2:1 $Si/Si_{0.4}Ge_{0.6}$ alloy superlattice [(red) curve with circles]. Experimental data from Ref. 19 are represented by the (blue) diamonds and (red) circles, while the data from Refs. 76 and 77 are given by the black squares. Dashed lines indicate the lattice thermal conductivity, while solid lines are the total thermal conductivity including the electronic contribution, which was calculated from the reported doping densities.

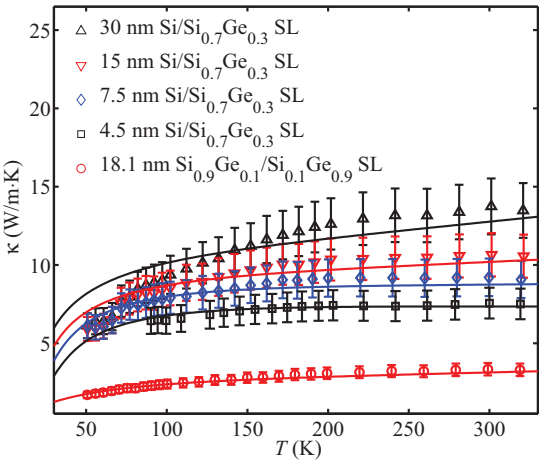

FIG. 7. (Color online) Cross-plane thermal conductivity of $Si/Si_{0.7}Ge_{0.3}$ alloy superlattices with period lengths of 4.5, 7.5, 15, and 30 nm [black squares, (blue) diamonds, (red) downward-pointing triangles, and black upward-pointing triangles, respectively), showing that the thermal conductivity in the presence of partially diffuse interface scattering scales with layer thickness, in agreement with the measurements and data reported in Ref. 19. In the case of the 18.1-nm $Si_{0.9}Ge_{0.1}/Si_{0.1}Ge_{0.9}$ superlattice [(red) circles], the presence of alloying in both layers of the superlattice and the large difference in the alloy concentration of the layers lead to a dramatic lowering of the thermal conductivity. All experimental data were taken from Ref. 19.

conductivity, κ_e, was calculated using the Wiedeman-Franz law and the reported measured carrier densities,[18,19] assuming an electron mobility value of $\mu_e = 100$ cm^2/Vs. Alloy films typically have very rough surfaces, so Δ was assumed to be 5 Å for both the 3.5-μm-thick $Si_{0.9}Ge_{0.1}$ film and the bulk-sintered $Si_{0.8}Ge_{0.2}$ alloy, while the 15-nm-period 2:1 $Si/Si_{0.4}Ge_{0.6}$ superlattice had a Δ of 1.85 Å, similar to the Si/Ge samples. The thermal conductivity of alloys reaches a minimum plateau for $x = 0.2$ (see Fig. 1) and typically cannot be reduced further by alloying alone. This was considered to be the "alloy limit." However, the 15-nm-period 2:1 $Si/Si_{0.4}Ge_{0.6}$ superlattice has a lower thermal conductivity than the bulk-sintered $Si_{0.8}Ge_{0.2}$ alloy, despite having the same relative proportions of Si and Ge (both contain 20% germanium because the ratio of the thicknesses of the Si and $Si_{0.4}Ge_{0.6}$ layers in the superlattice is 2:1). This reduction is explained by the additional scattering from the partially diffuse interfaces between layers of the superlattice, which acts in addition to the alloy scattering to reduce the thermal conductivity of the superlattice below that of the corresponding alloy with the same relative participation of Si and Ge. Therefore, we find that the alloy limit can be surpassed by utilizing diffuse interfaces.

Figure 7 shows a comparison between the model results and measurements from Ref. 19 for $Si/Si_{0.7}Ge_{0.3}$ alloy superlattices with period lengths of 4.5 nm, 7.5 nm, 15 nm, and 30 nm.[78] The 15-nm and 30-nm-period Si/SiGe superlattices have significantly higher thermal conductivities than the thinner samples shown in Fig. 7, owing to less influence of the roughness scattering. Our calculations accurately reproduce these experimental data from Ref. 19; however, we note that dislocation formation due to stress is quite possible in

large-period alloy superlattices[38] and has not been included in this model. Dislocation scattering would become more prominent at low temperatures. In the $Si/Si_{0.7}Ge_{0.3}$, the difference in the alloy composition of the two layers was small, leading to the small value of the rms interface roughness of 0.2 Å in our model. In contrast, when alloying is introduced in both layers and the difference in alloy concentration is large, as in the case of the 18.1-nm-period $Si_{0.9}Ge_{0.1}/Si_{0.1}Ge_{0.9}$ superlattice, the thermal conductivity is drastically reduced. The value of Δ is larger due to the larger lattice mismatch between layers. The value used here is 1.2 Å, very similar to the 15-nm-period $Si/Si_{0.4}Ge_{0.6}$ superlattice shown in Fig. 6, which also showed a similarly large difference in the alloy concentration of the two layers.

V. CONCLUSIONS

In summary, we have presented a model for the calculation of the full thermal conductivity tensor in $Si_{1-x}Ge_x/Si_{1-y}Ge_y$ superlattices based on solving the PBTE in the RTA. We have shown that the lifetime of phonons due to scattering with the rough interfaces depends not only on the thickness of each layer and the roughness of the interfaces, but also on the strength of the competing internal scattering mechanisms, such as isotope and phonon-phonon umklapp scattering. This competition between internal and interface scattering leads to a variation in the interface scattering rate between the case in which each layer is a single crystal and the case in which the structure contains alloys. The PBTE-RTA model captures the competing influences of internal and interface scattering mechanisms, which play out strongly in silicon/alloy and alloy/alloy superlattices. The model captures the anisotropy, temperature, and thickness variation of the measured samples reported in Refs. 17–19 and 41 very well.

Based on this model, we find that minimal thermal conductivity is achieved by introducing alloying into both layers in the superlattice and ensuring that the difference in the alloy concentration of the two layers is large. Further optimization is possible by reducing the overall thickness of the superlattice period, increasing the roughness of the interfaces, and either introducing alloying into both layers of the superlattice or minimizing the thickness of the pure layer in silicon-alloy superlattices. We also expect that superlattices with purely diffuse interfaces, such as those where quantum dots are present between layers,[79] will lead to a highly controllable thermal conductivity which scales with thickness.

ACKNOWLEDGMENTS

The authors thank S. Huxtable for helpful discussions regarding experiments in Refs. 18 and 19. Z.A.'s work on this project was funded by the NSF through the Computing Innovation Fellows Project (Grant No. 0937060 to the Computing Research Association, Sub-award No. CIF-146 to the University of Wisconsin) and by the CI TraCS Fellowship (Grant No. 1122690). I.K.'s work was funded by the AFOSR YIP program (Grant No. FA9550-09-1-0230) and by the NSF (Grant No. 1201311).

APPENDIX: ALLOY, ISOTOPE, AND UMKLAPP SCATTERING RATES

When two materials are combined in an alloy, such as in the case of $Si_{1-x}Ge_x$ considered here, the aperiodic mass variation between the two constituent types of atoms perturbs the lattice waves and leads to strong alloy scattering of phonons. Much like other point-defect scattering mechanisms, such as isotope and impurity, alloy scattering is elastic and has no temperature dependence.[80] The energy dependence of the alloy scattering rate is calculated from[81,82]

$$\frac{1}{\tau_{\text{Alloy}}(\omega)} = \frac{\pi}{6} V_0 \Gamma_{\text{Alloy}} \omega^2 D(\omega), \tag{A1}$$

where V_0 is the volume per atom and $D(\omega)$ is the vibrational density of states per unit volume.[83] The total energy-dependent vibrational density of states is given by a sum over all phonon branches b:

$$D(\omega) = \sum_{\text{b}} \int \frac{d\vec{q}}{(2\pi)^3} \delta[\omega - \omega_{\text{b}}(\vec{q})]. \tag{A2}$$

The volume integral of the energy-conserving δ function over the whole first Brillouin zone is calculated from the full phonon dispersion using the method of Gilat and Raubenheimer.[84]

The alloy disorder constant $\Gamma_{\text{Alloy}}(x)$ has three components—mass difference, isotope, and strain:

$$\Gamma_{\text{Alloy}}(x) = \Gamma_{\text{Mass}}(x) + \Gamma_{\text{Iso}} + \Gamma_{\text{Strain}}(x). \tag{A3}$$

The mass-difference constant $\Gamma_{\text{Mass}} = \sum_i f_i (1 - M_i/\overline{M})^2$, where f_i is the proportion of material i with mass M_i, while the average mass is $\overline{M} = \sum_i f_i M_i$.[85] The same expression also holds for isotope and impurity scattering within each material in the alloy.[86]

For the specific case of the $Si_{1-x}Ge_x$ alloy, the expression for Γ_{Mass} depends on the germanium fraction x in the alloy as

$$\Gamma_{\text{Mass}}(x) = x(1-x)\frac{(M_{\text{Ge}} - M_{\text{Si}})^2}{(x M_{\text{Ge}} + (1-x) M_{\text{Si}})^2}. \tag{A4}$$

The contribution due to isotopic variation in each of the constituent materials can be obtained by combining the isotope constants for each pure material as

$$\Gamma_{\text{Iso}}(x) = \frac{(1-x)\Gamma_{\text{Si}} M_{\text{Si}}^2 + x\Gamma_{\text{Ge}} M_{\text{Ge}}^2}{(x M_{\text{Ge}} + (1-x) M_{\text{Si}})^2}, \tag{A5}$$

where the pure silicon and germanium isotope scattering constants Γ_{Si} and Γ_{Ge} were taken from Ref. 85. An additional component to alloy scattering arising from the strain field due to the difference in lattice constants of pure Si and Ge and their alloys has been proposed. The contribution due to strain is then given by[87]

$$\Gamma_{\text{Strain}}(x) = \epsilon x(1-x)\frac{(a_{\text{Ge}} - a_{\text{Si}})^2}{a_{\text{SiGe}}^2(x)}, \tag{A6}$$

where $a_{\text{SiGe}}(x)$ is the composition-dependent alloy lattice constant, taken in the virtual crystal approximation, including bowing.[88] The empirical strain parameter is taken to be $\epsilon = 39$.[20] For most values of germanium concentration x, the strain contribution $\Gamma_{\text{Strain}}(x)$ is found to be much smaller than the mass-difference component.

The resistive umklapp phonon-phonon scattering rate was calculated in the standard general approximation for dielectric crystals,[85]

$$\tau_{b,U}^{-1}(\vec{q}) = \frac{\hbar\gamma_\lambda^2}{\overline{M}\Theta_b\bar{v}_\lambda^2}\omega_\lambda^2(\vec{q})Te^{-\Theta_\lambda/3T}, \quad \text{(A7)}$$

where the speed of sound $\bar{v}_b$ of each branch b is determined from the average slope of its dispersion curve near the Γ point, and $\overline{M}$ is the average atomic mass. The Grüneissen parameter γ_b was obtained for each branch from the phonon dispersion and has the value of 1.1 for the longitudinal acoustic branch and −0.6 for the transverse acoustic branch.[85] The expression in (A7) contains the exponential term $e^{-\Theta_b/3T}$ in the temperature dependence, which controls the onset of resistive umklapp scattering for each phonon branch through the branch-specific Debye temperatures Θ_λ, which were obtained from[89]

$$\Theta_b^2 = \frac{5\hbar^2}{3k_B^2}\frac{\int \omega^2 g_b(\omega)d\omega}{\int g_b(\omega)d\omega}, \quad \text{(A8)}$$

where the vibrational density of states function $g_b(\omega) = \sum_{b,\vec{q}} \delta[\omega - \omega_b(\vec{q})]$ was calculated for each phonon branch b from the full dispersion. This way, the temperature dependence of the contribution from each phonon branch to the total thermal conductivity is correctly represented.

*zlatana@engin.umass.edu
†knezevic@engr.wisc.edu

[1] F. J. DiSalvo, Science **285**, 703 (1999).
[2] C. J. Glassbrenner and G. A. Slack, Phys. Rev. **134**, A1058 (1964).
[3] P. Maycock, Solid-State Electron. **10**, 161 (1967).
[4] C. N. Liao, C. Chen, and K. N. Tu, J. Appl. Phys. **86**, 3204 (1999).
[5] A. Majumdar, Science **303**, 777 (2004).
[6] L. D. Hicks and M. S. Dresselhaus, Phys. Rev. B **47**, 12727 (1993).
[7] M. Dresselhaus, G. Chen, M. Tang, R. Yang, H. Lee, D. Wang, Z. Ren, J.-P. Fleurial, and P. Gogna, Adv. Mater. **19**, 1043 (2007).
[8] G. J. Snyder and E. S. Toberer, Nature Mater. **7**, 105 (2008).
[9] C. Bera, M. Soulier, C. Navone, G. Roux, J. Simon, S. Volz, and N. Mingo, J. Appl. Phys. **108**, 124306 (2010).
[10] G. Joshi, H. Lee, Y. Lan, X. Wang, G. Zhu, D. Wang, R. W. Gould, D. C. Cuff, M. Y. Tang, M. S. Dresselhaus, G. Chen, and Z. Ren, Nano Lett. **8**, 4670 (2008).
[11] A. J. Minnich, H. Lee, X. W. Wang, G. Joshi, M. S. Dresselhaus, Z. F. Ren, G. Chen, and D. Vashaee, Phys. Rev. B **80**, 155327 (2009).
[12] G. H. Zhu, H. Lee, Y. C. Lan, X. W. Wang, G. Joshi, D. Z. Wang, J. Yang, D. Vashaee, H. Guilbert, A. Pillitteri, M. S. Dresselhaus, G. Chen, and Z. F. Ren, Phys. Rev. Lett. **102**, 196803 (2009).
[13] R. Venkatasubramanian, E. Siivola, T. Colpitts, and B. O'Quinn, Nature **413**, 597 (2001).
[14] I. Chowdhury, R. Prasher, K. Lofgreen, G. Chrysler, S. Narasimhan, R. Mahajan, D. Koester, R. Alley, and R. Venkatasubramanian, Nature Nano. **4**, 235 (2009).
[15] E. Pop, Nano Res. **3**, 147 (2010).
[16] H. J. Ryu, Z. Aksamija, D. M. Paskiewicz, S. A. Scott, M. G. Lagally, I. Knezevic, and M. A. Eriksson, Phys. Rev. Lett. **105**, 256601 (2010).
[17] S.-M. Lee, D. G. Cahill, and R. Venkatasubramanian, Appl. Phys. Lett. **70**, 2957 (1997).
[18] S. T. Huxtable, A. R. Abramson, C.-L. Tien, A. Majumdar, C. LaBounty, X. Fan, G. Zeng, J. E. Bowers, A. Shakouri, and E. T. Croke, Appl. Phys. Lett. **80**, 1737 (2002).
[19] S. T. Huxtable, Ph.D. thesis, University of California, Berkeley, 2002.
[20] B. Abeles, Phys. Rev. **131**, 1906 (1963).
[21] P. Hyldgaard and G. D. Mahan, Phys. Rev. B **56**, 10754 (1997).
[22] M. V. Simkin and G. D. Mahan, Phys. Rev. Lett. **84**, 927 (2000).
[23] A. A. Kiselev, K. W. Kim, and M. A. Stroscio, Phys. Rev. B **62**, 6896 (2000).
[24] D. A. Broido and T. L. Reinecke, Phys. Rev. B **70**, 081310 (2004).
[25] S.-F. Ren, W. Cheng, and G. Chen, J. Appl. Phys. **100**, 103505 (2006).
[26] A. Ward and D. A. Broido, Phys. Rev. B **77**, 245328 (2008).
[27] S.-I. Tamura, Y. Tanaka, and H. J. Maris, Phys. Rev. B **60**, 2627 (1999).
[28] G. Chen, Phys. Rev. B **57**, 14958 (1998).
[29] B. Yang and G. Chen, Microscale Thermophys. Eng. **5**, 107 (2001).
[30] J. Garg and G. Chen, Phys. Rev. B **87**, 140302 (2013).
[31] I. O. Thomas and G. P. Srivastava, Phys. Rev. B **88**, 115207 (2013).
[32] L. Lindsay, D. A. Broido, and T. L. Reinecke, Phys. Rev. B **87**, 165201 (2013).
[33] G. Fugallo, M. Lazzeri, L. Paulatto, and F. Mauri, Phys. Rev. B **88**, 045430 (2013).
[34] I. Savić, D. Donadio, F. Gygi, and G. Galli, Appl. Phys. Lett. **102**, 073113 (2013).
[35] Y. Chalopin, K. Esfarjani, A. Henry, S. Volz, and G. Chen, Phys. Rev. B **85**, 195302 (2012).
[36] K.-H. Lin and A. Strachan, Phys. Rev. B **87**, 115302 (2013).
[37] M. Hu and D. Poulikakos, Nano Lett. **12**, 5487 (2012).
[38] A. Samarelli, L. F. Llin, S. Cecchi, J. Frigerio, T. Etzelstorfer, E. Müller, Y. Zhang, J. R. Watling, D. Chrastina, G. Isella, J. Stangl, J. P. Hague, J. M. R. Weaver, P. Dobson, and D. J. Paul, J. Appl. Phys. **113**, 233704 (2013).
[39] J. P. Dismukes, L. Ekstrom, E. F. Steigmeier, I. Kudman, and D. S. Beers, J. Appl. Phys. **35**, 2899 (1964).
[40] R. Cheaito, J. C. Duda, T. E. Beechem, K. Hattar, J. F. Ihlefeld, D. L. Medlin, M. A. Rodriguez, M. J. Campion, E. S. Piekos, and P. E. Hopkins, Phys. Rev. Lett. **109**, 195901 (2012).
[41] W. Liu, T. Borca-Tasciuc, G. Chen, J. Liu, and K. Wang, J. Nanosci. Nanotechnol. **1**, 39 (2001).
[42] P. Carruthers, Rev. Mod. Phys. **33**, 92 (1961).
[43] P. Klemens, *Solid State Physics* (Academic Press, New York, 1958).
[44] P. G. Klemens, Phys. Rev. **119**, 507 (1960).
[45] D. P. Sellan, J. E. Turney, A. J. H. McGaughey, and C. H. Amon, J. Appl. Phys. **108**, 113524 (2010).
[46] W. Weber, Phys. Rev. B **15**, 4789 (1977).
[47] Z. Aksamija and I. Knezevic, Phys. Rev. B **82**, 045319 (2010).
[48] P. Martin, Z. Aksamija, E. Pop, and U. Ravaioli, Phys. Rev. Lett. **102**, 125503 (2009).
[49] K. C. Rustagi and W. Weber, Solid State Commun. **18**, 673 (1976).

[50]D. Strauch and B. Dorner, J. Phys.: Condens. Matter **2**, 1457 (1990).
[51]B. D. Rajput and D. A. Browne, Phys. Rev. B **53**, 9052 (1996).
[52]M. C. Steele and F. D. Rosi, J. Appl. Phys. **29**, 1517 (1958).
[53]I. M. Khalatnikov and I. N. Adamenko, Zh. Eksp. Teor. Fiz. **63**, 746 (1972) [Sov. Phys. JETP **36**, 391 (1973)].
[54]P. L. Kapitza, Zh. Eksp. Teor. Fiz. **11**, 1 (1941) [J. Phys. USSR **4**, 181 (1941)].
[55]W. Eisenmenger, in *Phonon Scattering in Condensed Matter V*, edited by A. C. Anderson and J. P. Wolfe (Springer, Berlin, 1986).
[56]O. Weis, in *Nonequilibrium Phonons in Nonmetallic Crystals*, edited by W. Eisenmenger and A. A. Kaplyanskii (North-Holland, Amsterdam, 1986).
[57]E. T. Swartz and R. O. Pohl, Appl. Phys. Lett. **51**, 200 (1987).
[58]E. T. Swartz and R. O. Pohl, Rev. Mod. Phys. **61**, 605 (1989).
[59]G. Chen and M. Neagu, Appl. Phys. Lett. **71**, 2761 (1997).
[60]H. Zhao and J. B. Freund, J. Appl. Phys. **97**, 024903 (2005).
[61]E. S. Landry, M. I. Hussein, and A. J. H. McGaughey, Phys. Rev. B **77**, 184302 (2008).
[62]T. Borca-Tasciuc, W. Liu, J. Liu, T. Zeng, D. W. Song, C. D. Moore, G. Chen, K. L. Wang, M. S. Goorsky, T. Radetic, R. Gronsky, T. Koga, and M. S. Dresselhaus, Superlattices Microstruct. **28**, 199 (2000).
[63]B. Yang, W. L. Liu, J. L. Liu, K. L. Wang, and G. Chen, Appl. Phys. Lett. **81**, 3588 (2002).
[64]H. Zhao and J. B. Freund, J. Appl. Phys. **105**, 013515 (2009).
[65]S. B. Soffer, J. Appl. Phys. **38**, 1710 (1967).
[66]J. E. Turney, A. J. H. McGaughey, and C. H. Amon, J. Appl. Phys. **107**, 024317 (2010).
[67]J. Ziman, *Electrons and Phonons: The Theory of Transport Phenomena in Solids* (Oxford University Press, New York, 1960).
[68]E. H. Sondheimer, Adv. Phys. **1**, 1 (1952).
[69]G. Chen, J. Heat Transf. **119**, 220 (1997).
[70]G. Chen and T. Zeng, Microscale Thermophys. Eng. **5**, 71 (2001).
[71]J.-S. Heron, C. Bera, T. Fournier, N. Mingo, and O. Bourgeois, Phys. Rev. B **82**, 155458 (2010).
[72]J. S. Heron, T. Fournier, N. Mingo, and O. Bourgeois, Nano Lett. **9**, 1861 (2009).
[73]J. Alvarez-Quintana, E. Martínez, E. Pérez-Tijerina, S. A. Pérez-García, and J. Rodríguez-Viejo, J. Appl. Phys. **107**, 063713 (2010).
[74]S. Simons, J. Phys. C **7**, 4048 (1974).
[75]R. S. Prasher and P. E. Phelan, J. Heat Transf. **123**, 105 (2001).
[76]C. B. Vining, W. Laskow, J. O. Hanson, R. R. V. der Beck, and P. D. Gorsuch, J. Appl. Phys. **69**, 4333 (1991).
[77]D. G. Cahill, Thermal conductivity data (2011); available at: http://users.mrl.uiuc.edu/cahill/tcdata/tcdata.html.
[78]References 18 and 19 are based on the same measurements, but there is a small difference in the data analysis. Reference 19 is more recent and has been corrected for finite linewidth, as suggested in Ref. 90, which has resulted in a small downward shift of the thermal conductivity data with respect to the values reported in Ref. 18.
[79]G. Pernot, M. Stoffel, I. Savic, F. Pezzoli, P. Chen, G. Savelli, A. Jacquot, J. Schumann, U. Denker, I. Mnch, C. Deneke, O. G. Schmidt, J. M. Rampnoux, S. Wang, M. Plissonnier, A. Rastelli, S. Dilhaire, and N. Mingo, Nat. Mater. **9**, 491 (2010).
[80]D. A. Broido, A. Ward, and N. Mingo, Phys. Rev. B **72**, 014308 (2005).
[81]S.-I. Tamura, Phys. Rev. B **27**, 858 (1983).
[82]H. J. Maris, Phys. Rev. B **41**, 9736 (1990).
[83]J. Garg, N. Bonini, B. Kozinsky, and N. Marzari, Phys. Rev. Lett. **106**, 045901 (2011).
[84]G. Gilat and L. J. Raubenheimer, Phys. Rev. **144**, 390 (1966).
[85]D. T. Morelli, J. P. Heremans, and G. A. Slack, Phys. Rev. B **66**, 195304 (2002).
[86]W. Liu and M. Asheghi, J. Appl. Phys. **98**, 123523 (2005).
[87]B. Abeles, D. S. Beers, G. D. Cody, and J. P. Dismukes, Phys. Rev. **125**, 44 (1962).
[88]M. M. Rieger and P. Vogl, Phys. Rev. B **48**, 14276 (1993).
[89]G. Slack, *Solid State Physics, Vol. 34*, edited by F. Seitz, H. Ehrenreich, and D. Turnbull (Academic Press, New York, 1979).
[90]T. Borca-Tasciuc, A. R. Kumar, and G. Chen, Rev. Sci. Instrum. **72**, 2139 (2001).